Journal of the Optical Society of America B
OPTICAL PHYSICS

Splitting of a Tamm plasmon polariton at the interface between a metal and a resonant nanocomposite layer conjugated with a photonic crystal

Anastasia Yu. Avdeeva,[1,2,*] Stepan Ya. Vetrov,[2,1] and Ivan V. Timofeev[1,2]

[1]Kirensky Institute of Physics, Federal Research Center KSC SB RAS, Krasnoyarsk 660036, Russia
[2]Siberian Federal University, Krasnoyarsk 660041, Russia
*Corresponding author: Anastasia-yu-avdeeva@iph.krasn.ru

Received 26 January 2021; revised 28 March 2021; accepted 12 April 2021; posted 13 April 2021 (Doc. ID 420490); published 7 May 2021

Splitting of a Tamm plasmon polariton at the interface between a metal and a nanocomposite layer conjugated with a photonic crystal (Bragg mirror) has been theoretically investigated. The splitting can be implemented when the Tamm plasmon polariton frequency approaches the resonance frequency of the nanocomposite, which consists of metallic nanoballs dispersed in a transparent matrix. The reflectance spectrum of the *p*-polarized waves at the normal incidence of light has been calculated. It has been established that the Tamm plasmon polariton splitting significantly depends on the concentration of nanoballs in the nanocomposite layer and its thickness. The solution of the dispersion equation derived for a sample with semi-infinite mirrors has been compared with the spectra obtained for a finite structure by the transfer matrix method.

https://doi.org/10.1364/JOSAB.420490

1. INTRODUCTION

The optical Tamm state (OTS) is a surface state implemented at the interface between two media where multiple rereflections occur and light gets trapped between two mirrors [1,2]. The OTS is an optical analog of the electronic Tamm state, in which the electron density is localized at the boundary of the periodic potential of a crystal. This state can be excited at the interface between a photonic crystal (PC) and a metallic mirror. In this case, a light wave appears associated with the surface plasmon, i.e., oscillations of free electrons at the surface of a metal, and is called the Tamm plasmon polariton (TPP) [3–7]. In contrast to the surface plasmon, the TPP can be excited for both the *p* and *s* polarizations of light, even at its normal incidence onto the interface; the energy does not propagate along the interface, but exponentially decreases with the distance from the interface in both directions. The TPP manifests itself in experiments as a narrow resonance in the optical transmittance or reflectance spectrum of a sample at wavelengths within the photonic bandgap.

The TPPs have found application in fundamentally new devices, including absorbers [8], switches [9], lasers [10], white organic light-emitting diodes [11], heat emitters [12], sensors [13,14], and spontaneous emission amplifiers [15]. A high degree of field localization at the TPP frequency makes it possible to reduce the threshold of generation of nonlinear effects [16–18] and implement the extremely high light transmission through a nanohole [19].

The TPPs and devices based on them are formed, as a rule, using planar metallic films conjugated with a PC. In this case, the optimization of the optical properties of such structures via changing the parameters of the films is exhausted by choosing their material and thickness. New opportunities for optimizing the characteristics of the TPPs are offered by the use of resonant materials as structural elements. Such materials can be metal–dielectric nanocomposites (NCs), which consist of a dielectric matrix and metallic nanoballs uniformly distributed over its volume. The position and width of the NC resonance region, which lies in the visible spectral range, depend on the permittivity of initial materials and the concentration, size, and shape of nanoparticles. The effective characteristics of an NC consisting of metallic nanoparticles suspended in a dielectric matrix are formed by their plasmon resonance and, in the optical range, can take unique values atypical of natural materials [20–24]. The features of the spectral properties of the TPPs implemented at the interface between a PC and a metal–dielectric NC layer characterized by an effective resonance permittivity of $\varepsilon_{\text{mix}} < 0$ were explored in [25,26].

The aim of this study was to investigate the TPP localized at the interface between a metallic mirror and a resonant NC layer conjugated with a Bragg mirror. The TPP splitting effect is demonstrated and analyzed for the case when the NC resonance

frequency coincides with the TPP frequency or is similar to it. The possibility of controlling the position and number of Tamm modes by changing the parameters of the metal–dielectric NC layer is shown. It is established that the numerical solution of the dispersion equation for an unbounded sample is consistent with the reflectance spectrum obtained by the transfer matrix method for a bounded structure.

The application of the TPP splitting effect in the creation of a two-mode laser [10] and an organic solar cell [27] may be an incentive for experimental research of the new results obtained in this work. In [10], the generation of a single-mode laser with Tamm plasmon modes at the boundary of a multilayer dielectric structure and a metal was obtained. Due to the features of these modes, Tamma lasers open up prospects for the implementation of integrated microlasers. In [27], a structure comprising metal film-NC-PC is suggested as an organic solar cell. In such a structure, a TPP can be excited. An additional radiation absorption line appears in the active layer (NC layer) at the TPP wavelength. This mechanism of increasing the efficiency of organic solar cells was demonstrated.

2. DESCRIPTION OF THE MODEL

We consider a structure schematically shown in Fig. 1. The structure consists of a metallic layer, an NC layer, and a one-dimensional (1D) PC. The PC unit cell includes layers a and b with respective permittivities ε_a and ε_b and thicknesses d_a and d_b; the lattice period is $L = d_a + d_b$. The metallic layer has a permittivity ε_m. The NC with a thickness d is formed by metallic nanoballs dispersed in a transparent matrix and has an effective permittivity ε_{mix}. We assume that the medium surrounding the layered structure is vacuum.

To describe the optical properties of the NC layer, we use the effective medium approximation in the Maxwell–Garnett model, which is widely used in studying matrix media with a small volume fraction of isolated inclusions dispersed in the matrix material [28–30]:

$$\varepsilon_{\text{mix}} = \varepsilon_d \left[\frac{f}{(1-f)/3 + \varepsilon_d/(\varepsilon_m - \varepsilon_d)} + 1 \right], \tag{1}$$

where f is the filling factor, i.e., the fraction of nanoparticles in the matrix; ε_d and $\varepsilon_m(\omega)$ are the permittivities of the matrix and the nanoparticle metal; and ω is the radiation frequency. The size of inclusions is much smaller than the wavelength and depth of field penetration into the metal. We find the permittivity of the nanoparticle metal using the Drude–Sommerfeld approximation:

$$\varepsilon_m(\omega) = \varepsilon_0 - \frac{\omega_p^2}{\omega(\omega + i\gamma)}, \tag{2}$$

where ε_0 is the constant that takes into account the contributions of the interband transitions, ω_p is the plasmon frequency, and γ is the reciprocal electron relaxation time. The predictions of the Maxwell–Garnett effective medium model are reliable at a moderate fraction of inclusions with a filling factor of $f \ll 1$.

The $\varepsilon_{\text{mix}}(\omega)$ function is complex:

$$\varepsilon_{\text{mix}}(\omega) = \varepsilon'_{\text{mix}}(\omega) + i\varepsilon''_{\text{mix}}(\omega). \tag{3}$$

Ignoring the small factor γ^2, we find the resonance frequency position, which is determined by the characteristics of the initial materials and the dispersed phase concentration f:

$$\omega_0 = \omega_p \sqrt{\frac{1-f}{3\varepsilon_d + (1-f)(\varepsilon_0 - \varepsilon_d)}}. \tag{4}$$

At the point $\omega = \omega_0$, the function $\varepsilon'_{\text{mix}}(\omega)$ turns to zero, and the function $\varepsilon''_{\text{mix}}(\omega)$ takes the maximum value. In addition, the function $\varepsilon'_{\text{mix}}(\omega)$ turns to zero at the following point:

$$\omega_1 = \omega_p \sqrt{\frac{1+2f}{\varepsilon_0 + 2\varepsilon_d + 2f(\varepsilon_0 - \varepsilon_d)}}. \tag{5}$$

In the interval $[\omega_0, \omega_1]$, we have $\varepsilon'_{\text{mix}}(\omega) < 0$, i.e., in this frequency range, the NC is similar to the metal.

Figure 2(a) shows the real and imaginary parts of the dielectric constant of silver as functions of the wavelength. Figure 2(b) shows dispersion dependence of the NC permittivity at filling factors, $f = 0.01$.

3. DISPERSION EQUATIONS

The dispersion equation for a mode localized in an anisotropic layer embedded between a semi-infinite 1D PC and a metal was obtained in the general case in [31]. In the case of an embedded isotropic layer, the dispersion equation describing the TPP is reduced to the following form:

$$\frac{x e^{ik_a d_a} - r_{ab} e^{-ik_a d_a}}{x e^{-ik_b d_b} - r_{ab} e^{-ik_b d_b}} - \frac{e^{-ik_a d_a} - x r_{ab} e^{ik_a d_a}}{e^{ik_b d_b} - x r_{ab} e^{ik_b d_b}} = 0, \tag{6}$$

where

$$x = \frac{r_{\text{amix}} e^{-ik_{\text{mix}} d} - r_{\text{mmix}} e^{ik_{\text{mix}} d}}{e^{-ik_{\text{mix}} d} - r_{\text{mmix}} r_{\text{amix}} e^{ik_{\text{mix}} d}}, \tag{7}$$

and the wavenumbers in the corresponding layers are determined as

$$k_m = \frac{\omega}{c}\sqrt{\varepsilon_m}, \quad k_{\text{mix}} = \frac{\omega}{c}\sqrt{\varepsilon_{\text{mix}}}, \quad k_a = \frac{\omega}{c}\sqrt{\varepsilon_a},$$
$$k_b = \frac{\omega}{c}\sqrt{\varepsilon_b}, \tag{8}$$

while the Fresnel coefficients at the interfaces between the media are

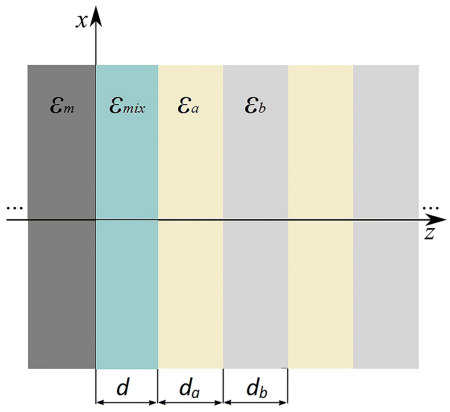

Fig. 1. Schematic of the investigated structure.

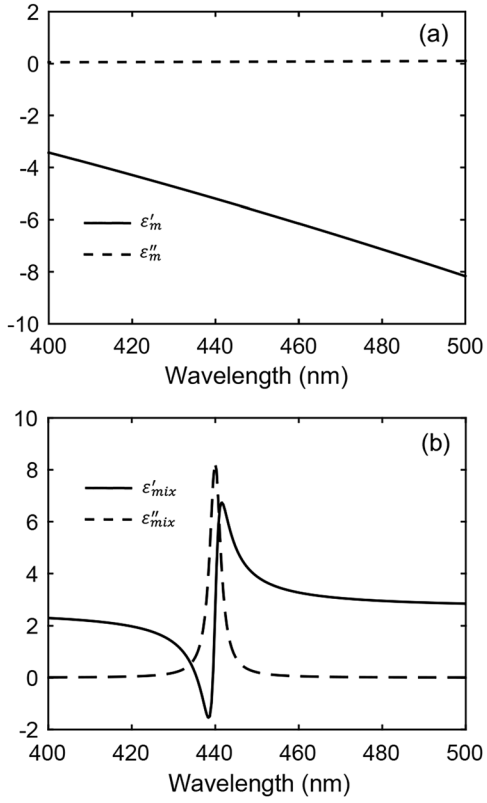

Fig. 2. (a) Real ε'_m and imaginary ε''_m parts of the ε_m versus wavelength. (b) Real $\varepsilon'_{\text{mix}}$ and imaginary $\varepsilon''_{\text{mix}}$ parts of the effective permittivity ε_{mix} versus wavelength. The permittivity of the NC matrix is set by the parameter $\varepsilon_d = 2.56$. The silver nanoballs with $\varepsilon_0 = 5$, $\hbar\omega p = 9$ eV, $\hbar\gamma = 0.02$ eV [33], and $f = 0.01$.

$$r_{\text{mmix}} = \frac{k_m - k_{\text{mix}}}{k_m + k_{\text{mix}}}, \quad r_{\text{amix}} = \frac{k_a - k_{\text{mix}}}{k_a + k_{\text{mix}}}, \quad r_{ab} = \frac{k_a - k_b}{k_a + k_b}. \tag{9}$$

The solution of Eq. (6) is the complex frequency $\omega = \omega_r + i\gamma$, whose real part determines the TPP spectral position.

4. TRANSFER MATRIX METHODS

The transmittance of a plane light wave polarized along the x axis and propagating in the z direction was calculated using the transfer matrix method [32]. The light field variation during passage through each structural layer is determined by the second-order transfer matrix. And the transfer matrix of the entire structure, which relates the amplitudes of the incident and outgoing waves, is calculated as the product of 2×2 matrices:

$$\hat{M} = \hat{T}_{01}\hat{T}_{12}\ldots\hat{T}_{N-1,N}\hat{T}_{N,S}, \tag{10}$$

where the transfer matrix is

$$T_{n-1,n} = \frac{1}{2}\begin{pmatrix} (1+h)e^{-i\alpha_n\gamma_n} & (1-h)e^{i\alpha_n\gamma_n} \\ (1-h)e^{-i\alpha_n\gamma_n} & (1+h)e^{i\alpha_n\gamma_n} \end{pmatrix}. \tag{11}$$

Here, $h = \sqrt{\varepsilon_n/\varepsilon_{n-1}}$, $\varepsilon(n)$ is the permittivity of the nth layer, $\alpha_n = (\omega/c)\sqrt{\varepsilon(n)}$, ω is the wave frequency, c is the speed of light, $\gamma_n = z_n - z_{n-1}$ $(n = 1, 2, \cdots, N)$ represents the layer thicknesses, and z_n is the coordinate of the interface between the nth layer and the $(n+1)$th layer adjacent from the right, $\gamma_{N+1} = 0$. The transfer matrix for the orthogonally polarized wave is obtained from Eq. (11) via the replacement of h by $\sqrt{\varepsilon_{n-1}/\varepsilon_n}$.

The energy transmittance, reflectance, and absorptance are expressed as

$$T(\omega) = \frac{1}{|\hat{M}_{11}|^2}, \quad R(\omega) = \frac{|\hat{M}_{21}|^2}{|\hat{M}_{11}|^2},$$
$$A(\omega) = 1 - T(\omega) - R(\omega), \tag{12}$$

where $\hat{M}_{11}$ and $\hat{M}_{22}$ are the elements of the matrix $\hat{M}$.

5. RESULTS AND DISCUSSIONS

In the absence of the metallic mirror and the NC layer, the bandgap of an unbounded PC lies in the wavelength range from 377.6 nm to 469.3 nm; the bandgap boundaries are shown by black horizontal lines in Figs. 3(a), 4(a), and 5. Red dotted lines superimposed over the reflectance spectrum represent the TPP

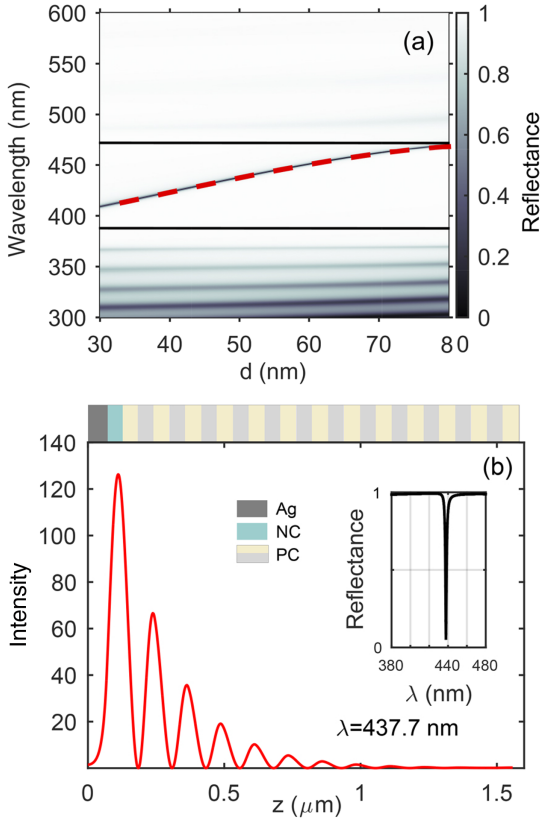

Fig. 3. (a) Reflectance spectrum of the investigated structure as a function of layer thickness d. The silver layer thickness in the structure is 70 nm; the PC length is 1.562 μm; the PC consists of 25 alternating ZrO_2 zirconium dioxide and SiO_2 silicon dioxide layers with thicknesses of $d_a = 74$ nm and $d_b = 50$ nm and refractive indices of $n_a = 1.45$ and $n_b = 2.04$; $\varepsilon_d = 2.56$; and the filling factor of the NC layer is $f = 0$. The red dashed curve corresponds to the solution of the dispersion equation for the TPP. The black horizontal lines correspond to the edges of the bandgap of the unbound PC. (b) Spatial distribution of the local field intensity in the sample normalized to the initial value corresponding to a TPP wavelength of $\lambda = 437.7$ nm. Inset, reflectance spectrum at $d = 50$ nm and $f = 0$.

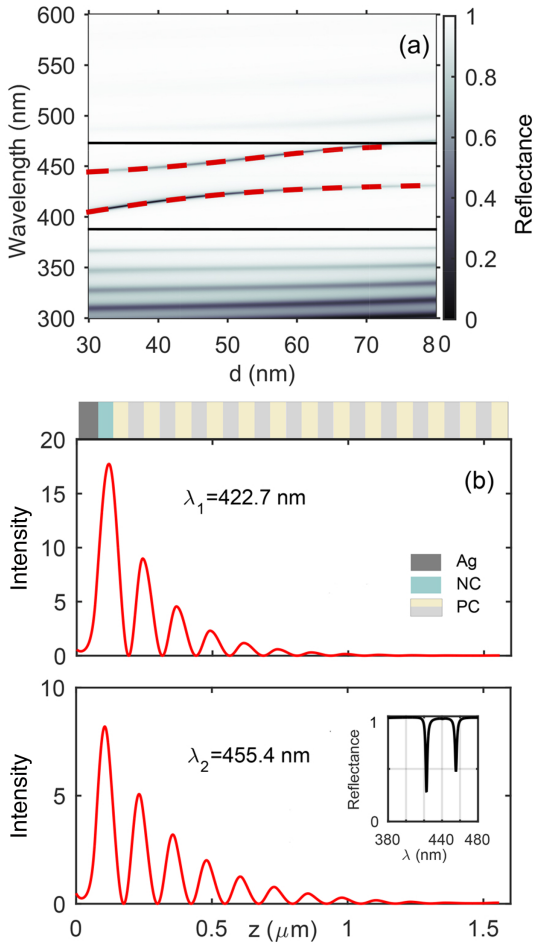

Fig. 4. (a) Reflectance spectrum of the investigated structure as a function of layer thickness d. The filling factor of the composite layer is $f = 0.01$; the other parameters are the same as in Fig. 3(a). Red dotted curves correspond to the solution of the dispersion equation for the TPP and black horizontal lines, to the boundaries of the bandgap of an unbounded PC. (b) Spatial distribution of the local field intensity in the sample normalized to the input value. Inset, reflectance spectrum at $d = 50$ nm and $f = 0.01$.

dispersion curves calculated by numerical solution of dispersion Eq. (6). Let us compare the obtained solution of the dispersion equation for the TPP localized in the sample with semi-infinite mirrors with the spectra calculated for a finite structure by the transfer matrix method.

In Fig. 3(a), it can be seen that the red dotted curve completely coincides with the gray solid curve, thereby demonstrating considerable agreement between the two calculation methods, even at a small number of PC periods. It should be noted that an increase in the number of PC layers improves the agreement of the solution of the dispersion equation at the PC bandgap edges. Upon increasing the layer thickness d, the phase of the reflection from the PC changes; the TPP frequency in the bandgap shifts to the long-wave region, which makes it possible to adjust the TPP position. In particular, at $d = 50$ nm, the TPP occurs at a wavelength of 437.7 nm, and the Q factor of the mode is 292. At $d = 80$ nm, the TPP frequency attains the upper limit of the PC bandgap and occurs at a wavelength of 468.8 nm.

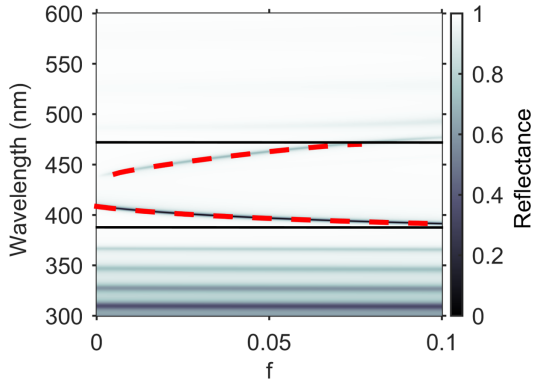

Fig. 5. Reflectance spectra of the investigated structure upon variation in filling factor f. At $d = 30$ nm, the rest of the parameters are the same as in Fig. 3(a). The red dashed line corresponds to the solution of the dispersion equation for the TPP. Black horizontal lines show the edges of the bandgap of an unbounded PC.

Figure 3(b) shows the spatial distribution of the local field intensity for the TPP frequency at $d = 50$ nm. The structure distribution of the electric field intensity normalized to the intensity of the incident light is colored in red. The field is localized in a region comparable with the wavelength.

When the NC layer is filled with metallic silver nanoballs with $\varepsilon_0 = 5$, $\hbar\omega p = 9$ eV, $\hbar\gamma = 0.02$ eV [33], the permittivity of the NC matrix is set by the parameter $\varepsilon_d = 2.56$; this permittivity is typical for some dense glasses, such as crown glass. The reflectance spectrum reveals the TPP frequency splitting effect [see Fig. 4(a)] for the case with $f = 0.01$, and the plasmon resonance frequency ω_0 is similar to the TPP frequency or coincides with it. Then, in contrast to the case $f = 0$ [Fig. 3(a)], there are two dips in the reflectance spectrum, which are caused by the ε_{mix} dispersion in the NC layer.

In addition, Fig. 4(a) shows excellent agreement between the curves obtained by solving the dispersion equation with the reflectance spectrum calculated by the transfer matrix method in the NC resonance region. Hence, it can be seen that the solution of the dispersion equation for the upper curve is limited by the edge of the bandgap of an infinite seed PC.

Figure 4(b) presents the spatial distribution of the local field intensity for the Tamm modes at wavelengths of $\lambda_1 = 422.7$ nm and $\lambda_2 = 455,4$ nm with Q factors of 201 and 207, respectively. Such wavelengths in the reflectance spectrum in Fig. 4(a) correspond to $d = 50$ nm. Consequently, the TPP splitting value is $\Delta\lambda = 32.4$ nm. Comparison of Figs. 3(b) and 4(b) shows that the maximum intensity decreased by an order of magnitude. It can be seen that the light is localized between the silver film and PC mirror and that the maximum of the local field strength is located in the NC layer and decreases exponentially in both directions.

Let us consider the effect of the concentration of nanoballs dispersed in the NC matrix on the reflectance spectrum. Figure 5 shows the reflectance spectra of the investigated structure at different volume fractions of nanoparticles in the NC layer at a concentration from 1% to 10%. It can be seen that, with a change in the f value, the high- and low-frequency modes are symmetrically repulsed and the splitting value increases with the concentration of silver nanoballs in the NC

layer. In particular, at $f = 0.05$, the TPP with a wavelength of 409 nm splits into two Tamm modes: a high-Q mode with $\lambda_1 = 397$ nm and a low-Q mode with $\lambda_2 = 463$ nm; in this case, the TPP splitting value is $\Delta\lambda = 66$ nm, which is twice as large as the splitting value at a concentration of 1%. Figure 5 shows good agreement between the curves obtained by solving numerically dispersion Eq. (7) with the reflectance spectrum of the structure calculated using the numerical method.

Equation (1) was obtained in the quasielectrostatic approximation, which is applicable when nanoparticles are much smaller than the wavelength in the medium. For the optical range, the thickness of the layers of a 1D PC is about a quarter of the radiation wavelength, which also imposes a restriction on the maximal size of nanoparticles. The size effect takes place when the average free path of the conduction electrons exceeds the size of the nanoparticles and the processes of scattering of electrons by the surface of a particle start to contribute considerably to relaxation. The collision of electrons with the surface of the nanoparticle is phenomenologically accounted for by introducing an additive to the relaxation rate inversely proportional to the radius r of the particle [34,35]:

$$\gamma = \gamma_0 + A\frac{V_f}{r}, \tag{13}$$

where $V_f = 1.4 \cdot 10^8$ sm/s is the velocity of electrons at the Fermi energy, r represents the nanoparticle radius, and A is

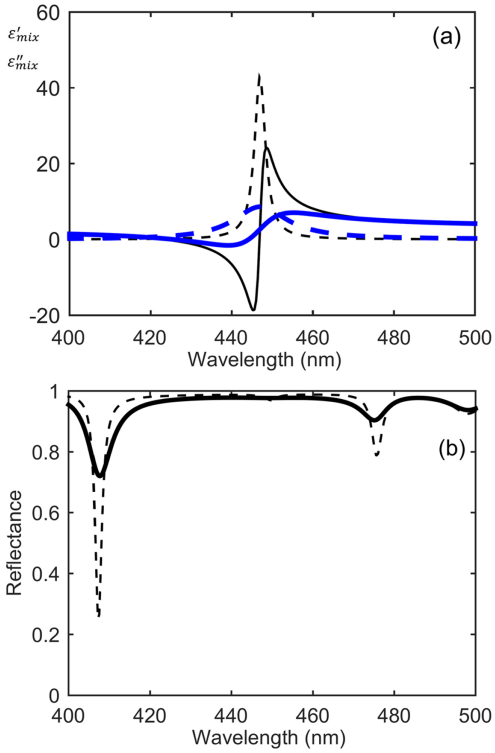

Fig. 6. (a) Real $\varepsilon'_{\text{mix}}$ (solid curve) and imaginary $\varepsilon''_{\text{mix}}$ (dashed curve) parts of the effective permittivity ε_{mix} NC at the filling factors $f = 0.05$—thin black lines without taking into account the particle size, thick blue lines at the $r = 7$ nm. (b) Reflectance spectra of the investigated structure at d = 60 nm and $f = 0.05$; the other parameters are the same as in Fig. 3(a). Dashed curve without taking into account the particle size, and the solid curve at the $r = 7$ nm, $A = 0.4$ [20].

the proportionality coefficient determined by the electron scattering at the nanoparticle surface.

The dependences in Fig. 6(a) show that the effective permittivity of the NC in the plasmon resonance region differs significantly from the values obtained without taking into account the size of nanoparticles. We note that the decrease in the nanoparticle size leads to the decrease in the amplitude values of the real and imaginary parts of the effective permittivity. At the same time, it can be seen from Fig. 6(b) that when taking into account the size adjustment, the TPP splitting effect is preserved.

6. CONCLUSION

Thus, the effect of TPP splitting at the interface between a metallic film and a resonant NC layer conjugated with a PC was demonstrated. It was shown that the TPP splitting is sensitive to the nanoparticle concentration and other parameters of an NC. The results obtained for a finite structure using the transfer matrix method were found to be in good agreement with the data determined by the independent method for solving the dispersion equation for an unbounded structure. The advantage of the proposed model is determined by the significantly extended possibility of effectively controlling the position of Tamm modes in the reflectance spectra of the PC structures via changing the parameters of the resonant NC layer. The significant dependence of the position of reflectance peaks on the NC layer thickness opens up the possibility of creating a tunable filter based on such a structure. To do this, it is necessary to fabricate an NC layer with a variable thickness, for example, wedge-shaped [36].

Funding. Russian Foundation for Basic Research (19-42-240004, 19-52-52006).

Acknowledgment. The reported study was funded by Russian Foundation for Basic Research, Government of Krasnoyarsk Territory, Krasnoyarsk Region Science and Technology Support Fund to the research project No. 19-42-240004 and by Russian Foundation for Basic Research, project No. 19-52-52006. The authors are thankful to Pavel S. Pankin for valuable discussions and comments.

Disclosures. The authors declare no conflicts of interest.

Data Availability. Data underlying the results presented in this paper are not publicly available at this time but may be obtained from the authors upon reasonable request.

REFERENCES

1. A. P. Vinogradov, A. V. Dorofeenko, A. M. Merzlikin, and A. A. Lisyansky, "Surface states in photonic crystals," Phys. Usp. **53**, 243–256 (2010).
2. A. V. Kavokin, I. A. Shelykh, and G. Malpuech, "Lossless interface modes at the boundary between two periodic dielectric structures," Phys. Rev. B **72**, 233102 (2005).
3. T. Goto, A. V. Dorofeenko, A. M. Merzlikin, A. V. Baryshev, A. P. Vinogradov, M. Inoue, A. A. Lisyansky, and A. B. Granovsky, "Optical Tamm states in one-dimensional magnetophotonic structures," Phys. Rev. Lett. **101**, 113902 (2008).
4. M. Kaliteevski, I. Iorsh, S. Brand, R. A. Abram, J. M. Chamberlain, A. V. Kavokin, and I. A. Shelykh, "Tamm plasmon-polaritons: possible electromagnetic states at the interface of a metal and a dielectric Bragg mirror," Phys. Rev. B **76**, 165415 (2007).

5. B. I. Afinogenov, V. O. Bessonov, I. V. Soboleva, and A. A. Fedyanin, "Ultrafast all-optical light control with Tamm plasmons in photonic nanostructures," ACS Photon. **6**, 844–850 (2019).
6. H.-C. Cheng, C.-Y. Kuo, Y.-J. Hung, K.-P. Chen, and S.-C. Jeng, "Liquid-crystal active Tamm-plasmon devices," Phys. Rev. Appl. **9**, 064034 (2018).
7. A. Valitova, A. Koryukin, A. Gazizov, and M. K. Salakhov, "Improving the surface layer structure in opal-like plasmonic-photonic crystals for efficient excitation of optical Tamm states," Opt. Mater. **110**, 110404 (2020).
8. Y. Gong, X. Liu, H. Lu, L. Wang, and G. Wang, "Perfect absorber supported by optical Tamm states in plasmonic waveguide," Optics Express **19**, 18393–18398 (2011).
9. W. Zhang and S. Yu, "Bistable switching using an optical Tamm cavity with a Kerr medium," Opt. Commun. **283**, 2622–2626 (2010).
10. C. Symonds, A. Lematre, P. Senellart, M. H. Jomaa, S. A. Guebrou, E. Homeyer, G. Brucoli, and J. Bellessa, "Lasing in a hybrid GaAs/silver Tamm structure," Appl. Phys. Lett. **100**, 121122 (2012).
11. X.-L. Zhang, J. Feng, X.-C. Han, Y.-F. Liu, Q.-D. Chen, J.-F. Song, and H.-B. Sun, "Hybrid Tamm plasmon-polariton/microcavity modes for white top-emitting organic light-emitting devices," Optica **2**, 579–584 (2015).
12. Z. Y. Yang, S. Ishii, T. Yokoyama, T. D. Dao, M. G. Sun, T. Nagao, and K. P. Chen, "Tamm plasmon selective thermal emitters," Opt. Lett. **41**, 4453–4456 (2016).
13. P. S. Maji, M. K. Shukla, and R. Das, "Blood component detection based on miniaturized self-referenced hybrid Tamm-plasmon-polariton sensor," Sens. Actuators B Chem. **255**, 729–734 (2018).
14. X. Zhang, X.-S. Zhu, and Y.-W. Shi, "An optical fiber refractive index sensor based on the hybrid mode of Tamm and surface plasmon polaritons," Sensors **18**, 2129 (2018).
15. A. R. Gubaydullin, C. Symonds, J. Bellessa, K. A. Ivanov, E. D. Kolykhalova, M. E. Sasin, A. Lemaitre, P. Senellart, G. Pozina, and M. A. Kaliteevski, "Enhancement of spontaneous emission in Tamm plasmon structures," Sci. Rep. **7**, 9014 (2017).
16. A. P. Vinogradov, A. V. Dorofeenko, S. G. Erokhin, M. Inoue, A. A. Lisyansky, A. M. Merzlikin, and A. B. Granovsky, "Surface state peculiarities in one-dimensional photonic crystal interfaces," Phys. Rev. B **74**, 045128 (2006).
17. C. H. Xue, H. T. Jiang, H. Lu, G. Q. Du, and H. Chen, "Efficient third-harmonic generation based on Tamm plasmon polaritons," Opt. Lett. **38**, 959–961 (2013).
18. B. I. Afinogenov, V. O. Bessonov, and A. A. Fedyanin, "Second-harmonic generation enhancement in the presence of Tamm plasmon-polaritons," Opt. Lett. **39**, 6895–6898 (2014).
19. I. V. Treshin, V. V. Klimov, P. N. Melentiev, and V. I. Balykin, "Optical Tamm state and extraordinary light transmission through a nanoaperture," Phys. Rev. A **88**, 023832 (2013).
20. V. Klimov, *Nanoplasmonics* (Jenny Stanford, 2014).
21. A. N. Oraevsky and I. E. Protsenko, "Optical properties of heterogeneous media," Quantum Electron. **31**, 252–256 (2001).
22. S. V. Sukhov, "Nanocomposite material with the unit refractive index," Quantum Electron. **35**, 741–744 (2005).
23. S. G. Moiseev, "Active Maxwell–Garnett composite with the unit refractive index," Phys. B **405**, 3042–3045 (2010).
24. S. Y. Vetrov, A. Y. Avdeeva, and I. V. Timofeev, "Spectral properties of a one-dimensional photonic crystal with a resonant defect nanocomposite layer," J. Exp. Theor. Phys. **113**, 755–761 (2011).
25. S. Y. Vetrov, R. Bikbaev, and I. V. Timofeev, "The optical Tamm states at the edges of a photonic crystal bounded by one or two layers of a strongly anisotropic nanocomposite," Opt. Commun. **395**, 275–281 (2017).
26. S. Y. Vetrov, R. G. Bikbaev, and I. V. Timofeev, "Optical Tamm states at the interface between a photonic crystal and a nanocomposite with resonance dispersion," J. Exp. Theor. Phys. **117**, 988–998 (2013).
27. X.-L. Zhang, J.-F. Song, X.-B. Li, J. Feng, and H.-B. Sun, "Optical Tamm states enhanced broad-band absorption of organic solar cells," Appl. Phys. Lett. **101**, 243901 (2012).
28. J. C. M. Garnett, "XII. Colours in metal glasses and in metallic films," Philos. Trans. R. Soc. London, Ser. A **203**, 385–420 (1904).
29. L. A. Golovan, V. Y. Timoshenko, and P. K. Kashkarov, "Optical properties of porous-system-based nanocomposites," Phys. Usp. **50**, 595–612 (2007).
30. A. Sihvola, *Electromagnetic Mixing Formulas and Applications* (IET, 1999).
31. P. S. Pankin, B.-R. Wu, J.-H. Yang, K.-P. Chen, I. V. Timofeev, and A. F. Sadreev, "One-dimensional photonic bound states in the continuum," Commun. Phys. **3**, 91 (2020).
32. P. Yeh, "Electromagnetic propagation in birefringent layered media," J. Opt. Soc. Am. **69**, 742–756 (1979).
33. P. B. Johnson and R. W. Christy, "Optical constants of the noble metals," Phys. Rev. B **6**, 4370–4379 (1972).
34. V. Y. Reshetnyak, I. P. Pinkevych, T. J. Sluckin, A. M. Urbas, and D. R. Evans, "Effective medium theory for anisotropic media with plasmonic core-shell nanoparticle inclusions," Eur. Phys. J. Plus **133**, 373 (2018).
35. S. G. Moiseev, V. A. Ostatochnikov, and D. I. Sementsov, "Influence of size effects on the optical characteristics of a one-dimensional photonic crystal with a nanocomposite defect," JETP Lett. **100**, 371–375 (2014).
36. R. Brückner, M. Sudzius, S. I. Hintschich, H. Fröb, V. G. Lyssenko, and K. Leo, "Hybrid optical Tamm states in a planar dielectric microcavity," Phys. Rev. B **83**, 033405 (2011).